**Supplementary Figure 1**

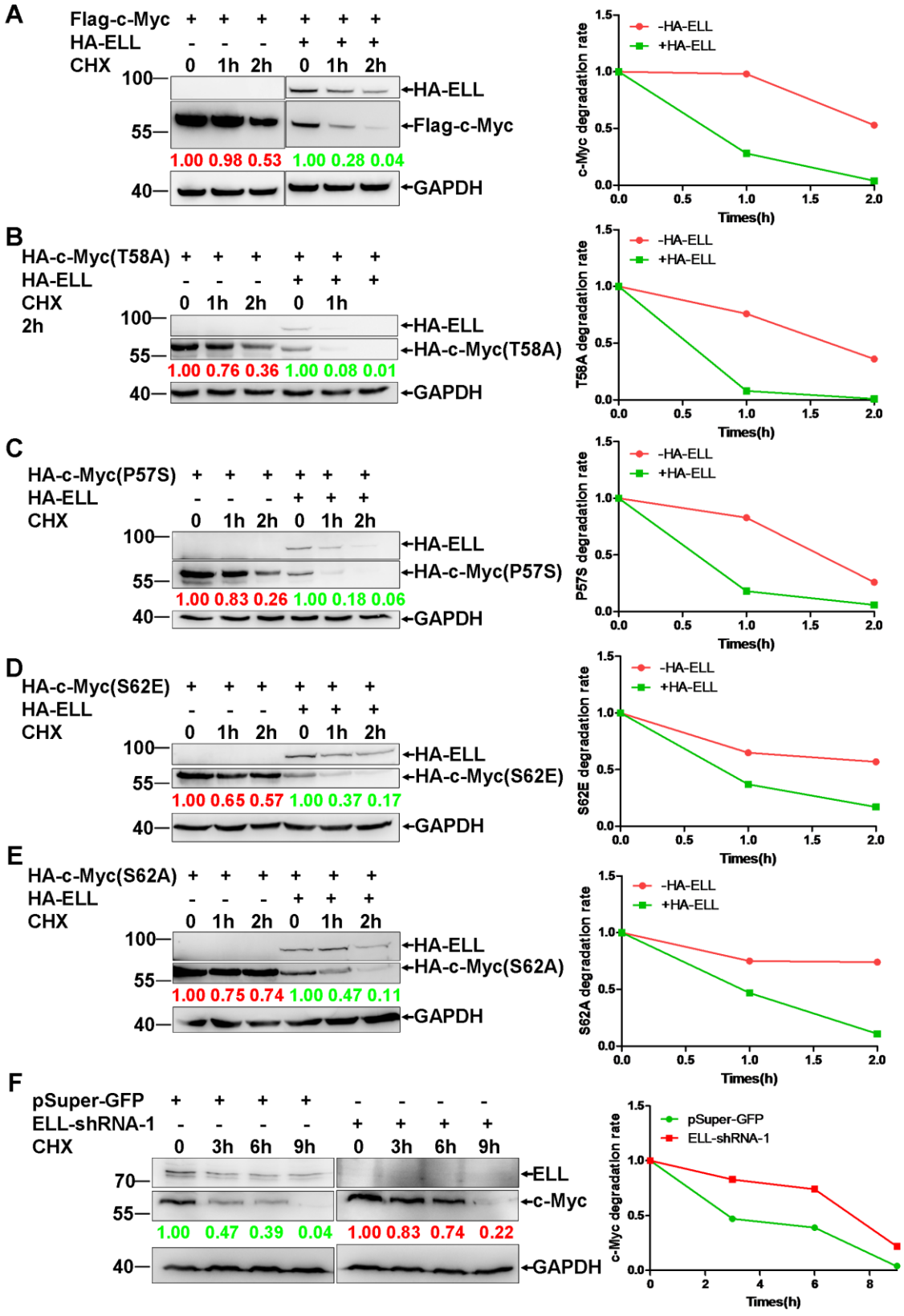

**Supplementary Fig. 1. ELL Induces c-Myc Degradation.** (A) Overexpression of HA-ELL in HEK293 cells promotes Flag-c-Myc degradation in the presence of cycloheximide (CHX, 50μg/mL). (B-E) Overexpression of HA-*ELL* in HEK293 cells promotes degradation of c-Myc mutants, HA-c-Myc(T58A) (B), HA-c-Myc(P57S) (C), HA-c-Myc(S62E) (D), and HA-c-Myc(S62A) (E), in the presence of cycloheximide (CHX, 50μg/mL). (F) Knockdown of ELL in HCT116 cells via ELL-shRNA-1 enhances the stability of endogenous c-Myc protein level in the presence of cycloheximide (CHX, 50μg/mL).

**Supplementary Figure 2**

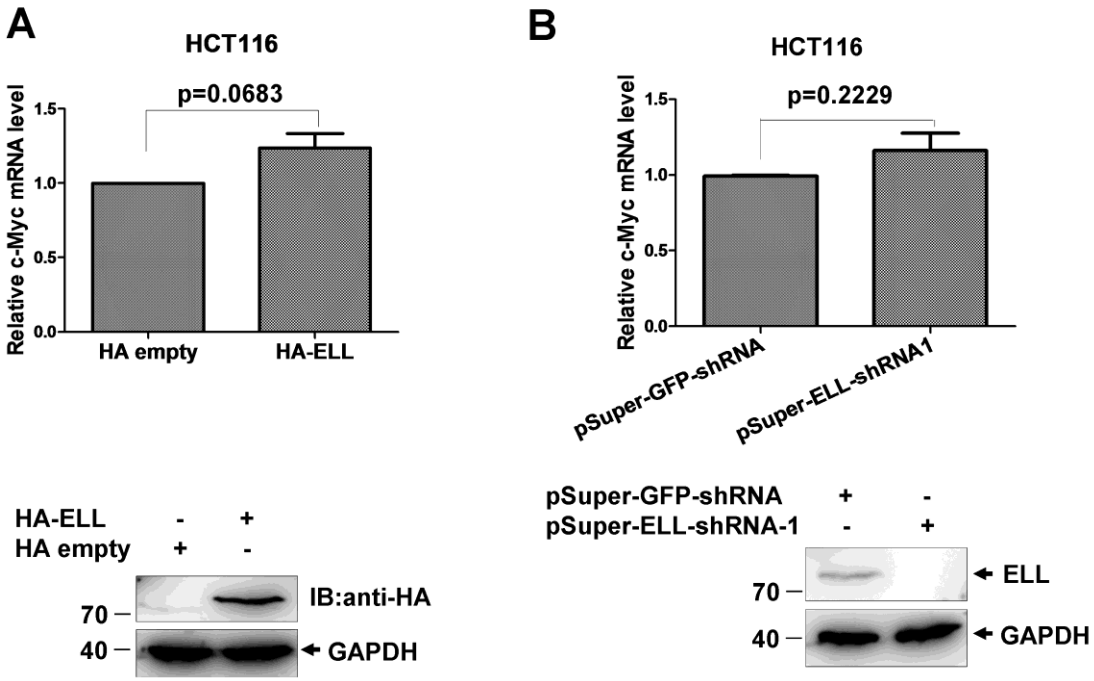


**Supplementary Fig. 2. ELL has no obvious effect on the transcription of *c-Myc*. (A)** Overexpression of ELL in HCT116 cells does not change *c-Myc* mRNA level as revealed by semi-quantitative RT-PCR assays (p=0.0683, *t*-test). (B) Knockdown of ELL in HCT116 cells does not change *c-Myc* mRNA level as revealed by semi-quantitative RT-PCR assays (p=0.2229, *t*-test).

**Supplementary Figure 3**

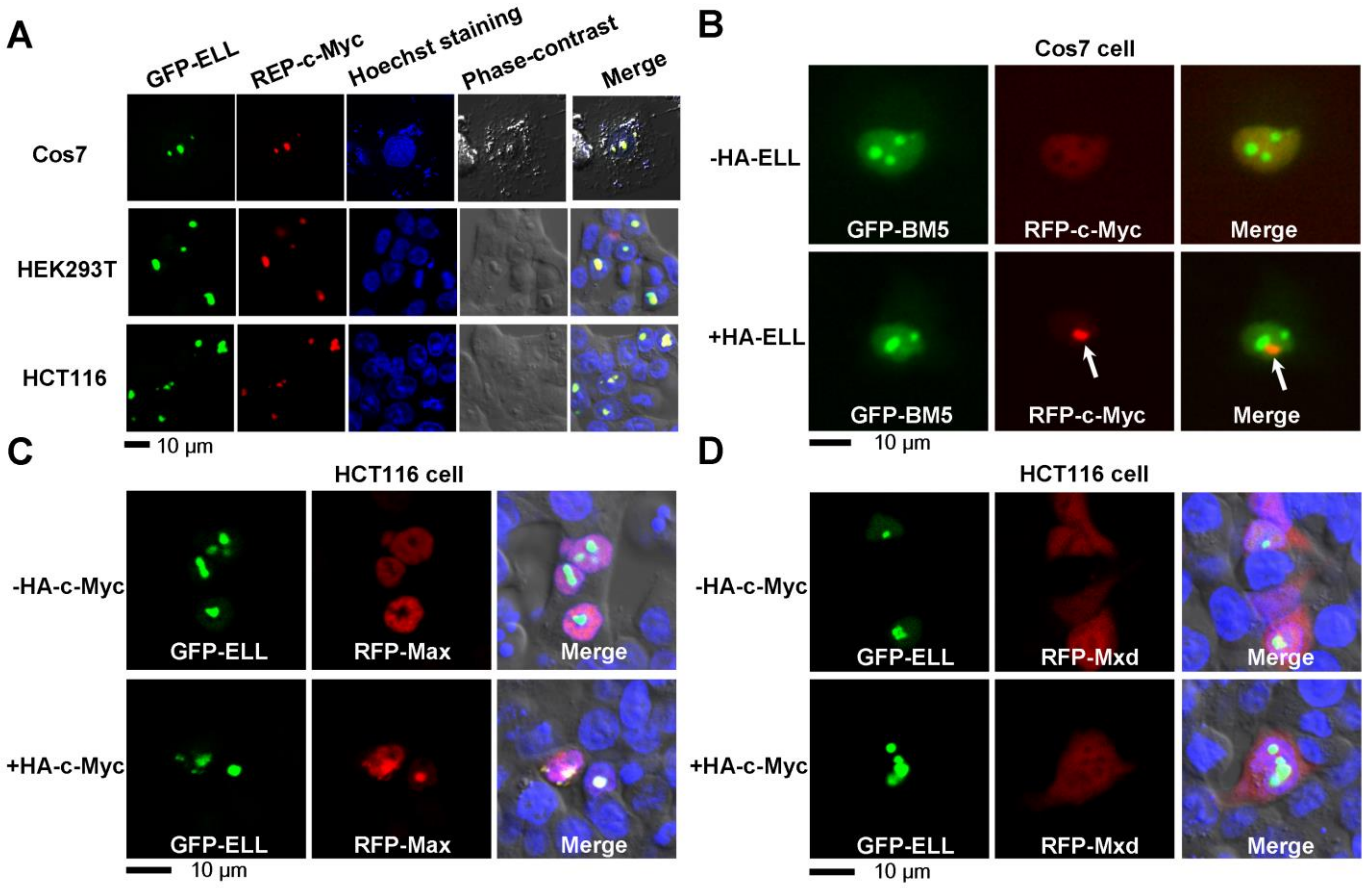


**Supplementary Fig. 3. ELL and c-Myc do not co-localize in the nuclei but co-localize in c-Myc/Max complex.** (A) GFP-ELL co-localizes with RFP-c-Myc in the nuclei of Cos7, HEK293T and HCT116 cells. (B) In the absence of HA-ELL, RFP-c-Myc does not localize to the nucleolus, which is marked by GFP-tagged BM5 (upper panels) in Cos7 cells. In the presence of HA-ELL, RFP-c-Myc is concentrated to form a speckle in the nucleus of Cos7 cells (white arrow), but not at the nucleolus as marked by GFP-BM5 (lower panels). (C) In the absence of HA-c-Myc, GFP-ELL localizes in the nuclei of HCT116 cells, but not co-localizes with RFP-Max (upper panels). In the presence of HA-c-Myc, GFP-ELL and RFP-Max co-localizes in the nuclei of HCT116 cell (lower panels). (D) In the absence/presence of HA-c-Myc, GFP-ELL does not co-localize with RFG-Mxd.

**Supplementary Figure 4**

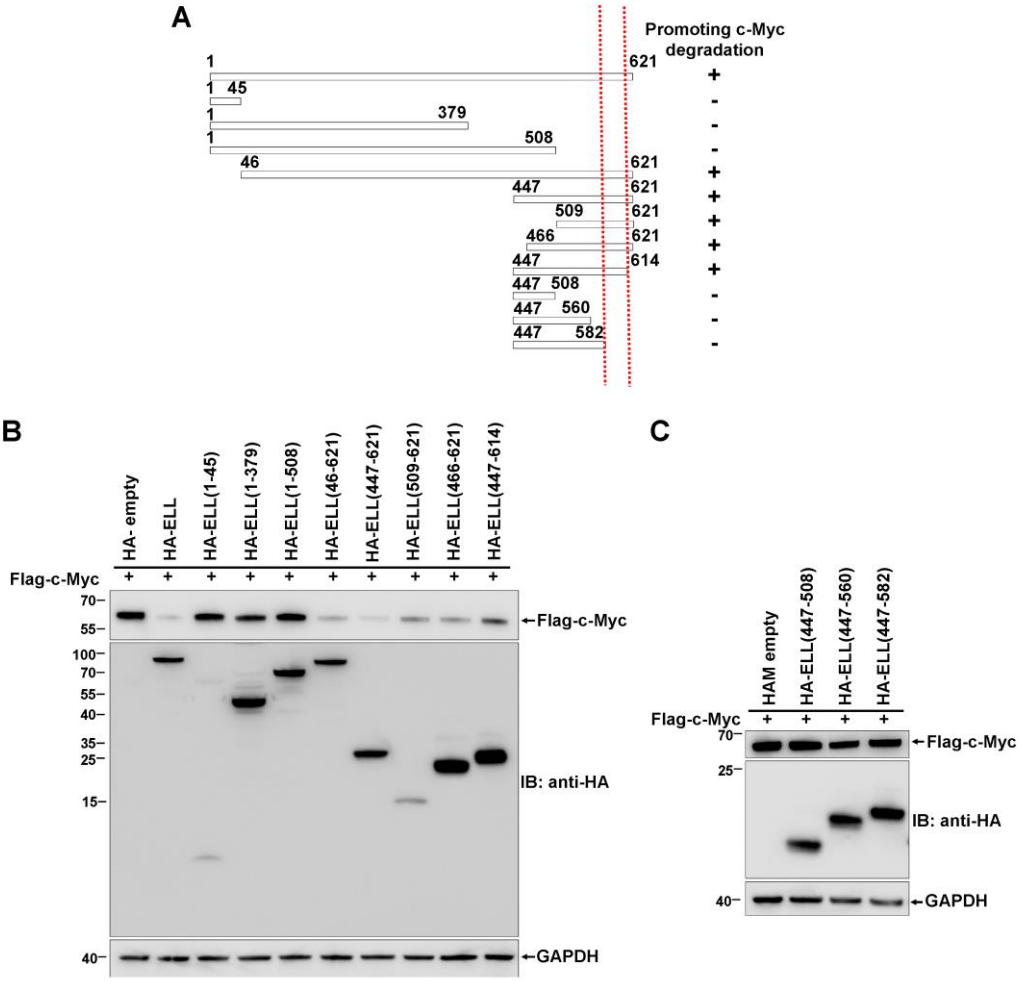


**Supplementary Fig. 4. Domain mapping of ELL for promoting c-Myc degradation**. (A) Schematic of ELL domains. The truncated domain promoting c-Myc degradation is indicated by plus sign (+); the region (aa 583-614) in ELL required for promoting c-Myc degradation is marked by two red-dash lines. (B, C) The effect of ELL domains on c-Myc degradation is examined by Western blot analysis; Flag-c-Myc is co-transfected with the indicated plasmids in HEK293 cells.

**Supplementary Figure 5**

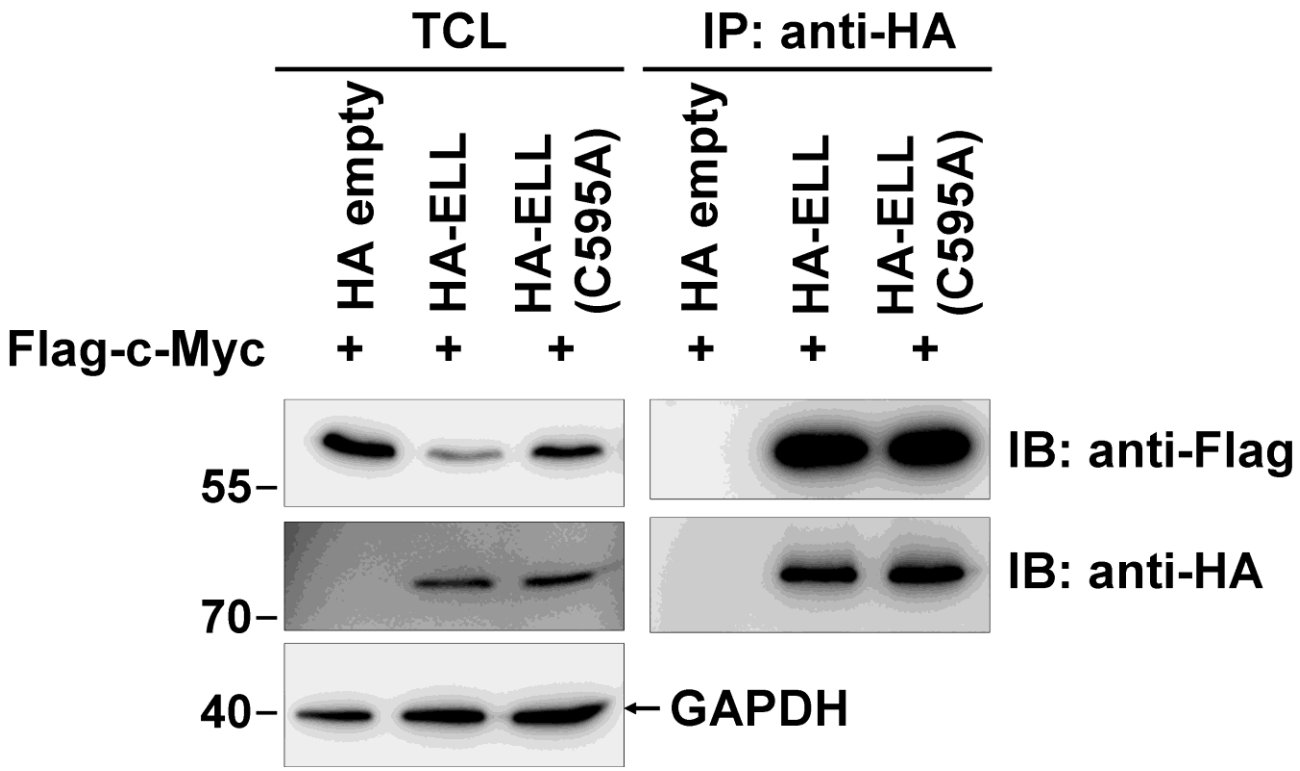


**Supplementary Fig. 5. Interaction of c-Myc with ELL mutant** (A) Co-immunoprecipitation of human c-Myc with the HA-ELL(C595A) mutant in HEK293T cells transfected with the indicated plasmids.

**Supplementary Figure 6**

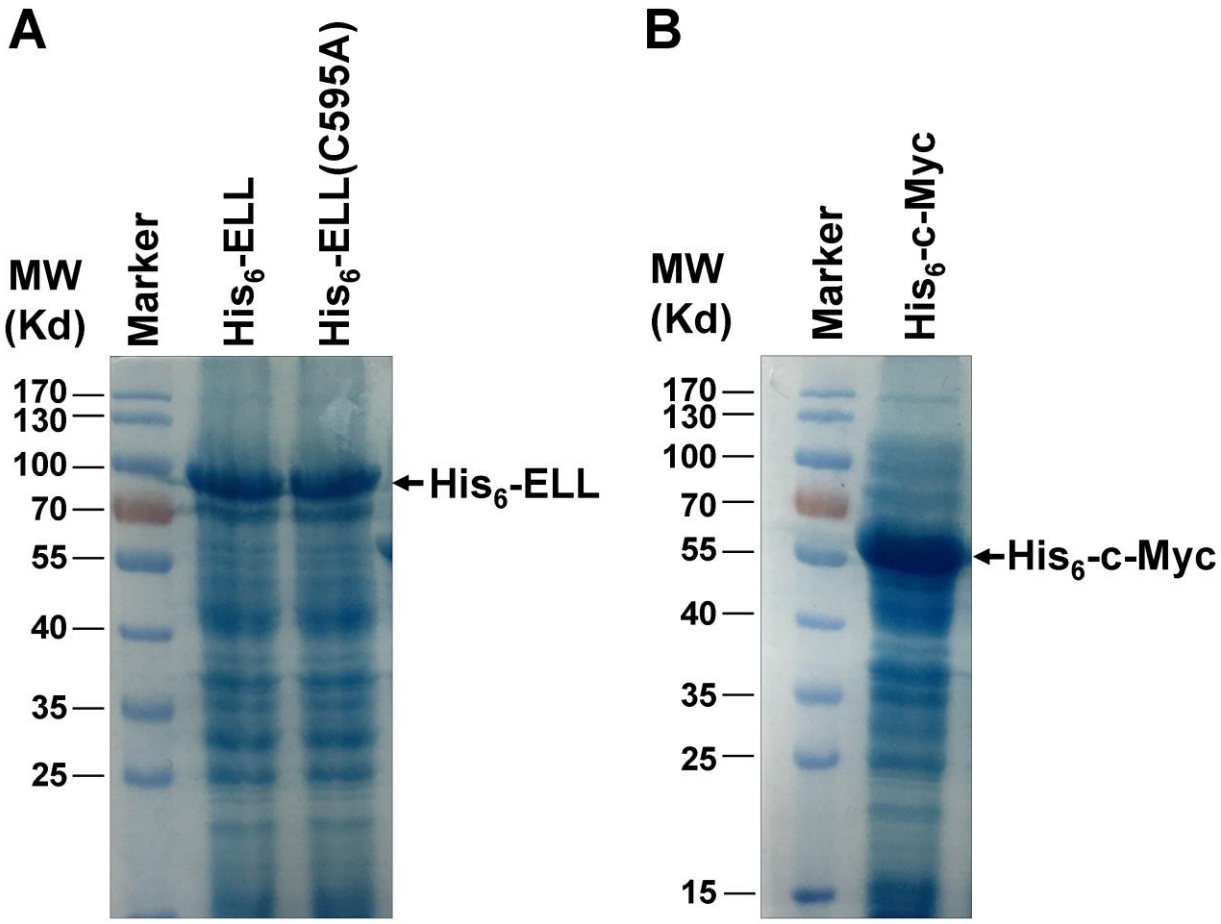


**Supplementary Fig. 6. Bacterial expression of His6-ELL, His6-ELL(C595A) and His6-c-Myc..**

(A) His6-ELL and His6-ELL(C595A) purified from *E. coli* extracts are examined by SDS-PAGE. (B) His6-c-Myc purified from *E. coli* extracts is examined by SDS-PAGE.

**Supplementary Figure 7**

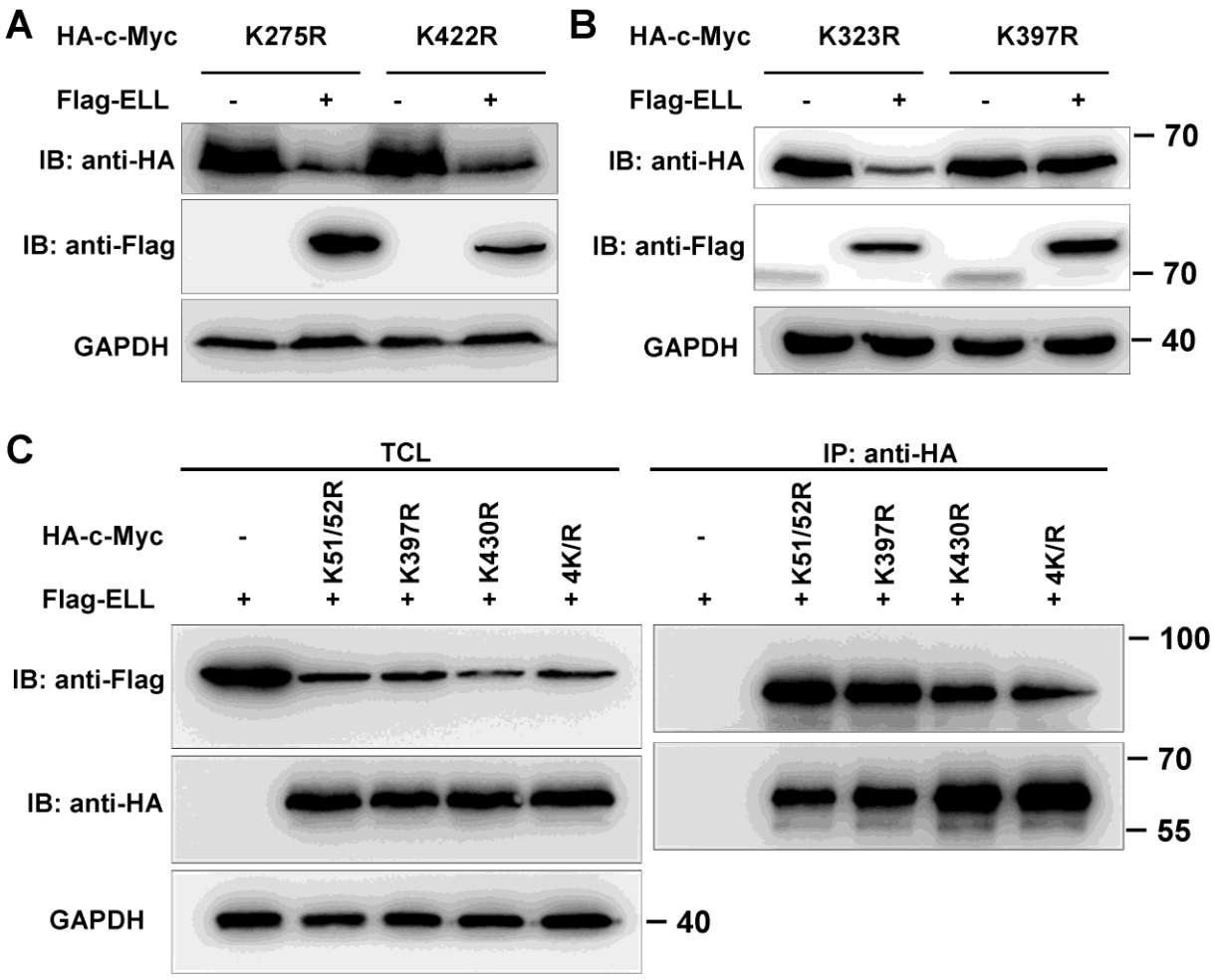


**Supplementary Fig. 7. Analysis of ELL-induced degradation and interaction with c-Myc mutants.** (A) ELL-induced degradation of K275R and K422R c-Myc mutants is further confirmed. (B) ELL does not induce K397R degradation, but indeed induce K323R degradation. (C) Co-immunoprecipitation of human ELL with the human c-Myc mutants, K51/52R, K397R, K430R and 4K/R, in HEK293T cells transfected with the indicated plasmids.

## Supplementary Figure 8

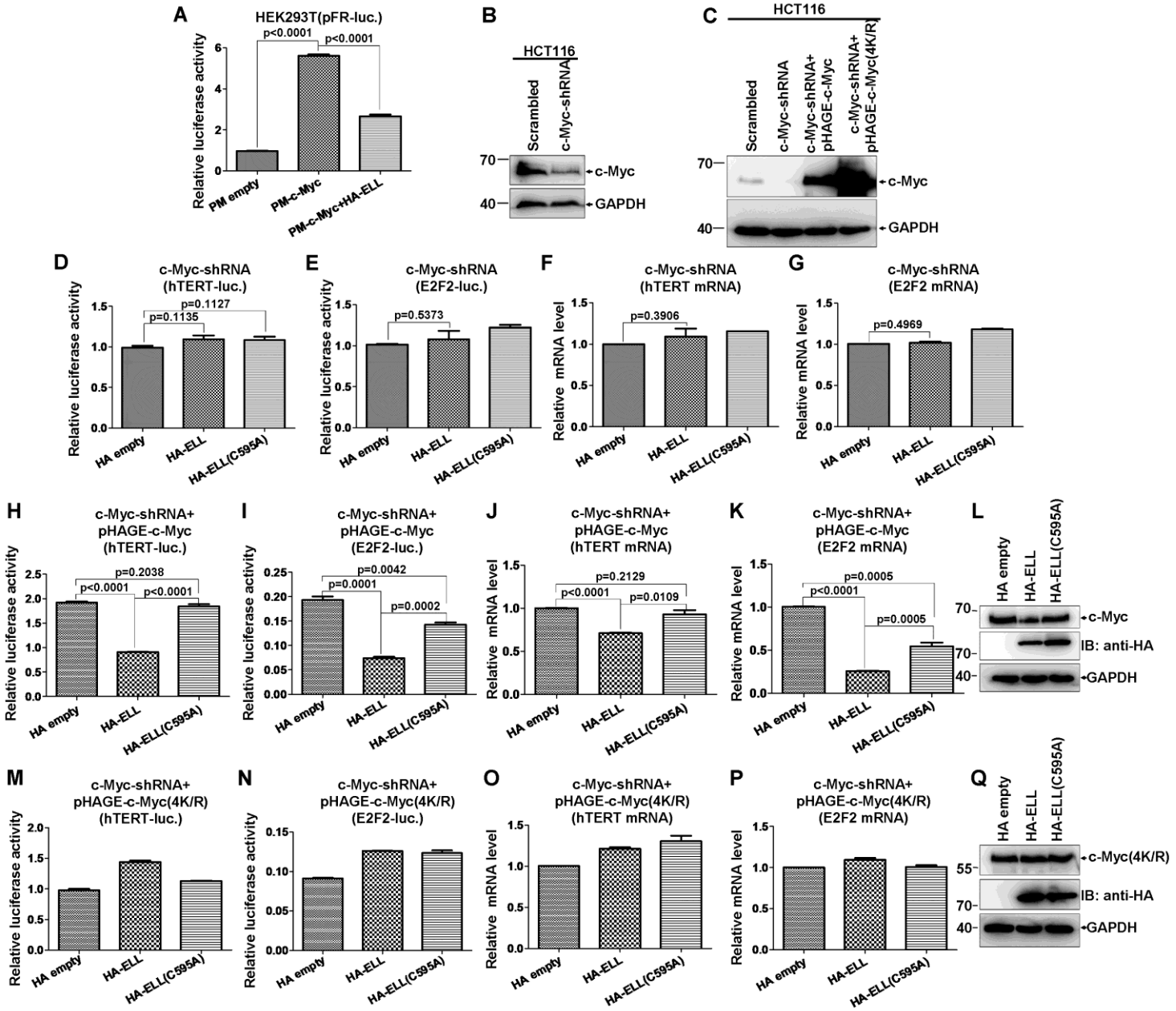

**Supplementary Fig. 8. c-Myc is required for ELL-mediated inhibition of downstream targets of *c-Myc*.** (A) Overexpression of ELL suppresses c-Myc transcriptional activity. (B) shRNA-mediated knockdown of c-Myc via lentivirus infection in HCT116 cells is confirmed by Western blot analysis. (C) Knockdown of c-Myc and overexpression of wild-type c-Myc or c-Myc(4K/R) mutant is confirmed by Western blot analysis. (D, E) Overexpression of HA-ELL or HA-ELL(C-595A) has no effect on *hTERT* (D) and *E2F2* (E) promoter reporter activity in HCT116 cells after c-Myc knockdown. (F, G) Overexpression of HA-ELL has no effect on *hTERT* (F) and *E2F2* (G) mRNA level in HCT116 cells after c-Myc knockdown. (H, I) The inhibitory effect of ELL on *hTERT* (H) and *E2F2* (I) promoter reporter activity is restored when wild-type c-Myc is re-expressed in HCT116 cells after c-Myc knockdown. (J, K) The inhibitory effect of ELL on *hTERT* (J) and *E2F2* (K) mRNA level is restored when wild-type c-Myc is re-expressed in HCT116 cells after c-Myc knockdown. (L) Overexpression of HA-ELL, HA-ELL(C595A) and c-Myc is confirmed by Western blot analysis. (M, N) The inhibitory effect of ELL on *hTERT* (M) and *E2F2* (N) promoter reporter activity is not restored when the c-Myc(4K/R) mutant is expressed in HCT116 cells after c-Myc knockdown. (O, P) The suppressive effect of ELL on *hTERT* (O) and *E2F2* (P) mRNA level is not restored when c-Myc(4K/R) mutant is expressed in HCT116 cells after c-Myc knockdown. (Q) Overexpression of HA-ELL, HA-ELL(C595A) and c-Myc (4K/R) is confirmed by Western blot analysis. Data are presented as mean ±SEM of three independent experiments performed in triplicate. The statistical analysis was performed using GraphPad Prism 5 (unpaired t-test).

**Supplementary Figure 9**

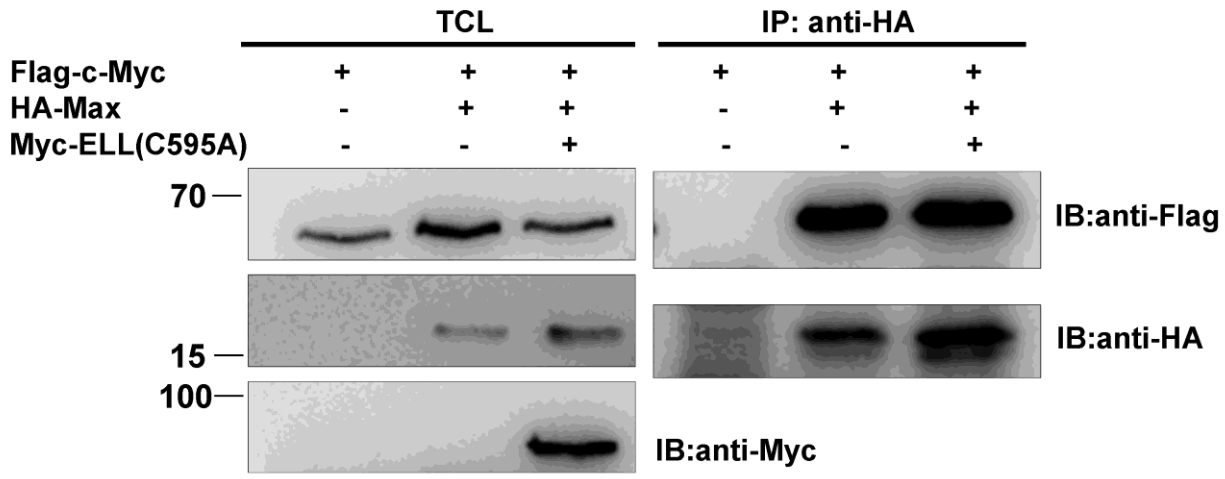


**Supplementary Fig. 9. ELL has no obvious effect on the interaction between c-Myc and Max**.

Co-immunoprecipitation of c-Myc with Max in HEK293T cells transfected with the indicated plasmids.

**Supplementary Figure 10**

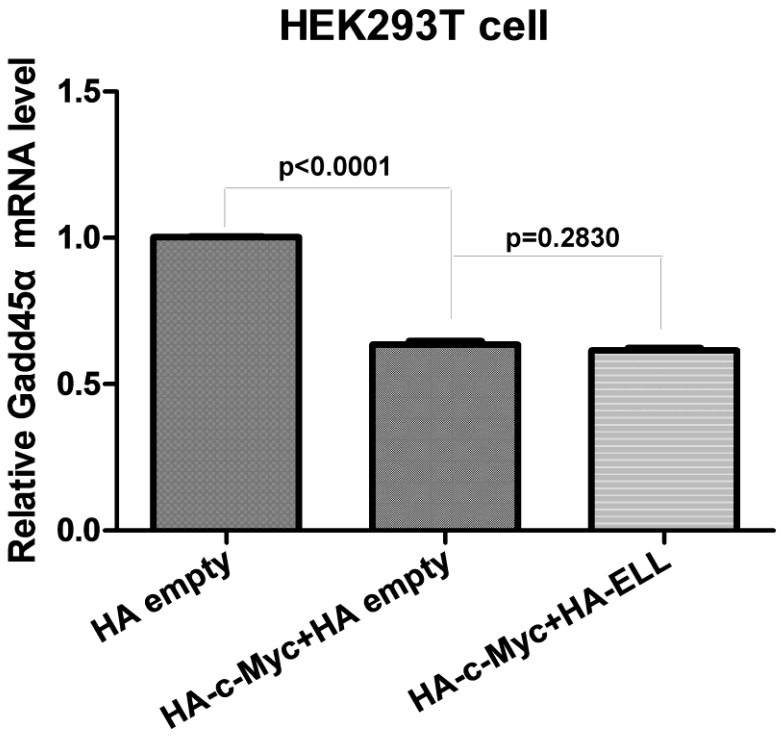


**Supplementary Fig. 10. ELL has no effect on c-Myc suppressive function.** c-Myc inhibits Gadd45α expression ($p<0.0001$, *t*-test), but co-transfection of ELL with c-Myc has no obvious effect on c-Myc suppressive function ($p=0.2830$, *t*-test) in HEK293T cells as revealed by semi-quantitative RT-PCR analysis.

**Supplementary Figure 11**

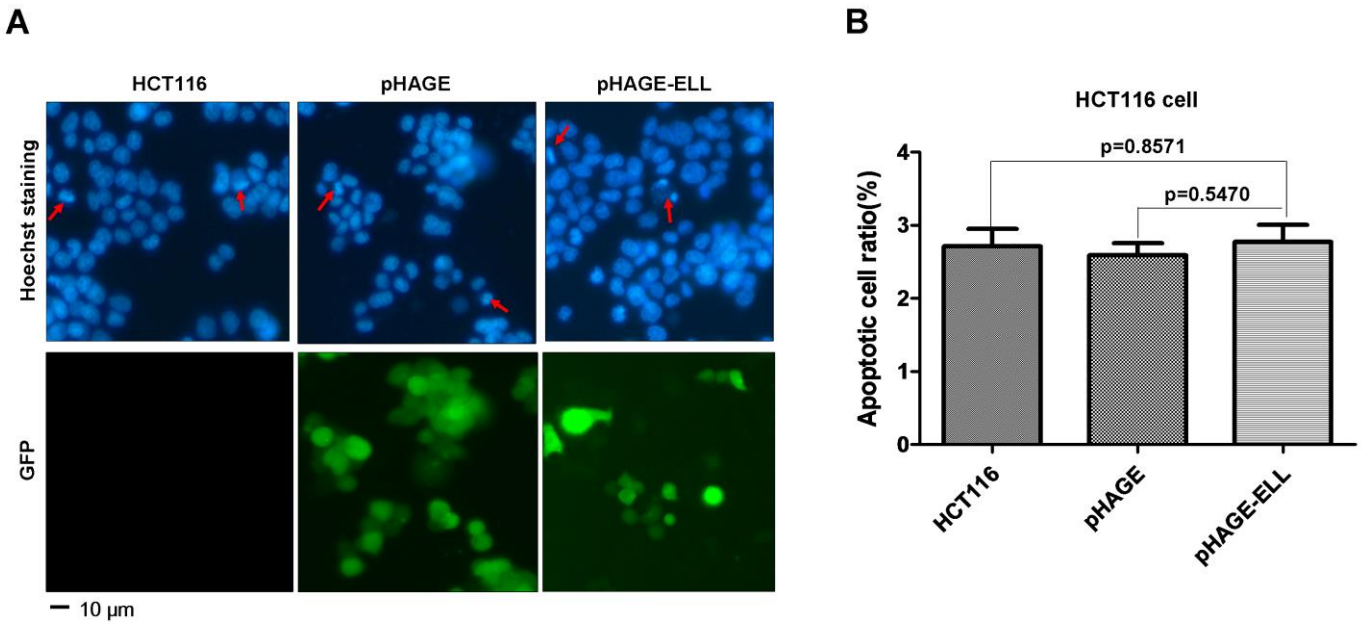


**Supplementary Fig. 11. ELL has no effect on cell apoptosis.** (A) HCT116 parental cells, HCT116 cells infected with lentivirus control and HCT116 cells infected with ELL-overexpression lentivirus were stained by Hoechst 33342, and the apoptotic cells were countered based on the photographs taken under a fluorescence microscope. (B) quantitative analysis for apoptotic cells. Data are presented as mean ±SEM performed in triplicate. The statistical analysis was performed using GraphPad Prism 5 (unpaired t-test)

**Supplementary Figure 12**

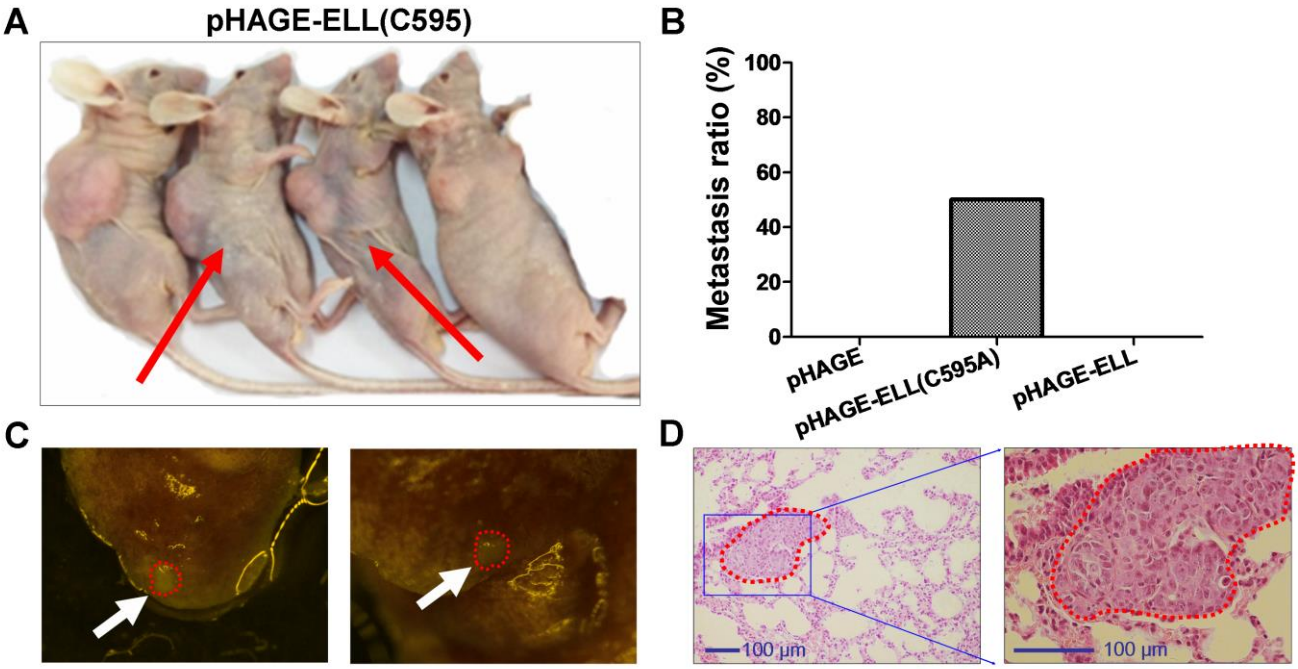


**Supplementary Fig. 12. The ELL (C595A) mutant promotes colon cancer metastasis in nude mice.** (A) Nude mice with ELL(C595A)-expressing HCT116 xenograft tumors exhibits cachexia (red arrow).(B) quantitative analysis for metastasis ratio. (C) Macro-metastasis (red-dashed circle; white arrow) are observed in the lungs of nude mice (the red arrows marked in A) with ELL(C595A)-expressing tumors. (D) The metastasis in the lungs of nude mice with ELL(C595A)-expressing tumors is confirmed by histological analysis after hematoxyin and eosin staining (red-dashed circle).

**Supplementary Figure 13**

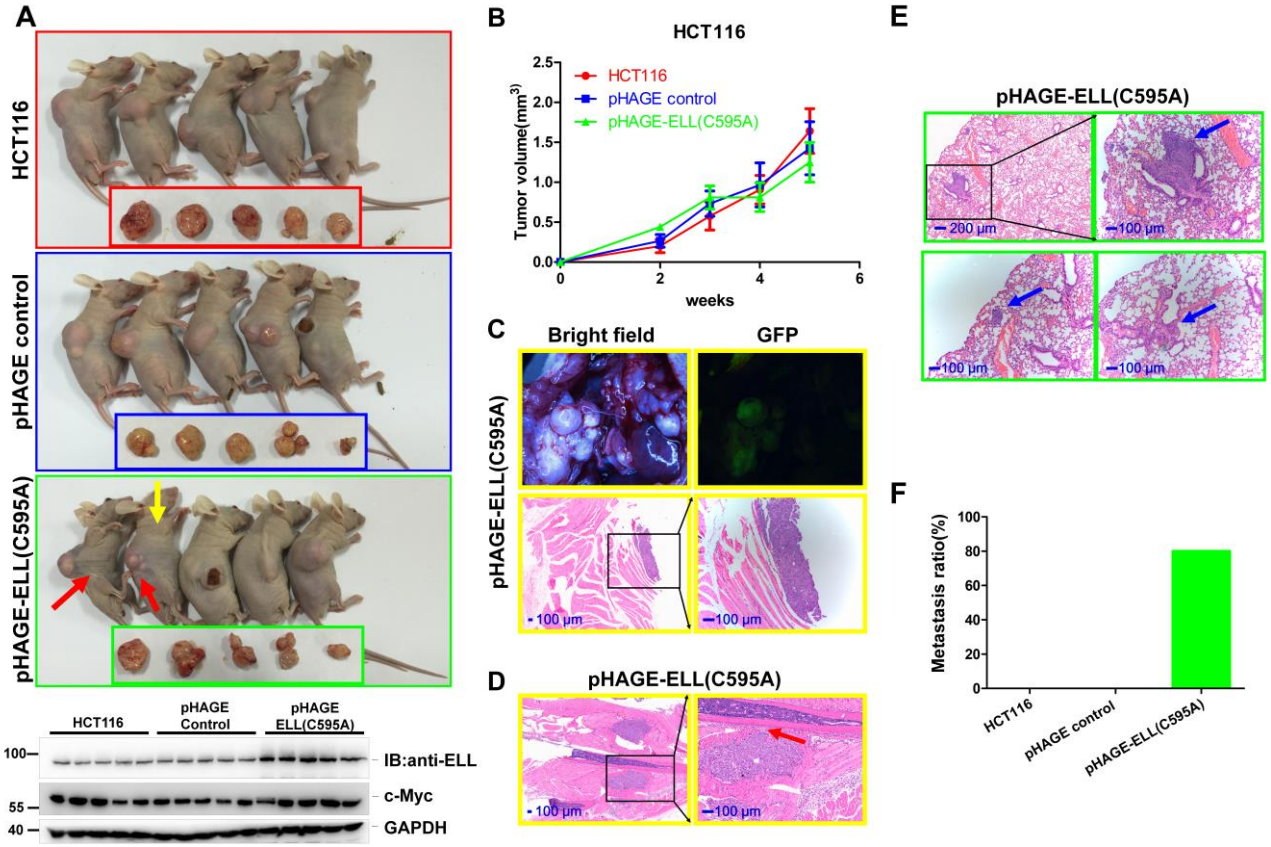


**Supplementary Fig. 13. The xenograft tumors derived from HCT116 parental cells, pHAGE control cells and pHAGE-ELL(C595A) cells have similar growth rate, and the ELL (C595A) mutant promotes colon cancer metastasis is further confirmed. (A)** The xenograft tumors derived from HCT116 parental cells, pHAGE control cells and pHAGE-ELL(C595A) cells. Two mice with pHAGE-ELL(C595A) tumor exhibit cachexia (red arrows). (**B**) The growth rates of xenograft tumors derived from HCT116 parental cells, pHAGE control cells and pHAGE-ELL(C595A) cells. (**C**) One mice (yellow arrow in A) developed macro-metastasis in the whole chest. The tumor cells are labeled by GFP expression as a result of Lentivirus infection (pHAGE vector contains a GFP marker). (**D**) the mice (yellow arrow in A) with macro-metastasis in the chest exhibits potential bone invasion. (**E**) the micro-metastasis developed in the lung of other three mice with pHAGE-ELL(C595A) is detected by histological analysis (blue arrows). (**F**) quantitative analysis for metastasis ratio.

**Supplementary Figure 14**

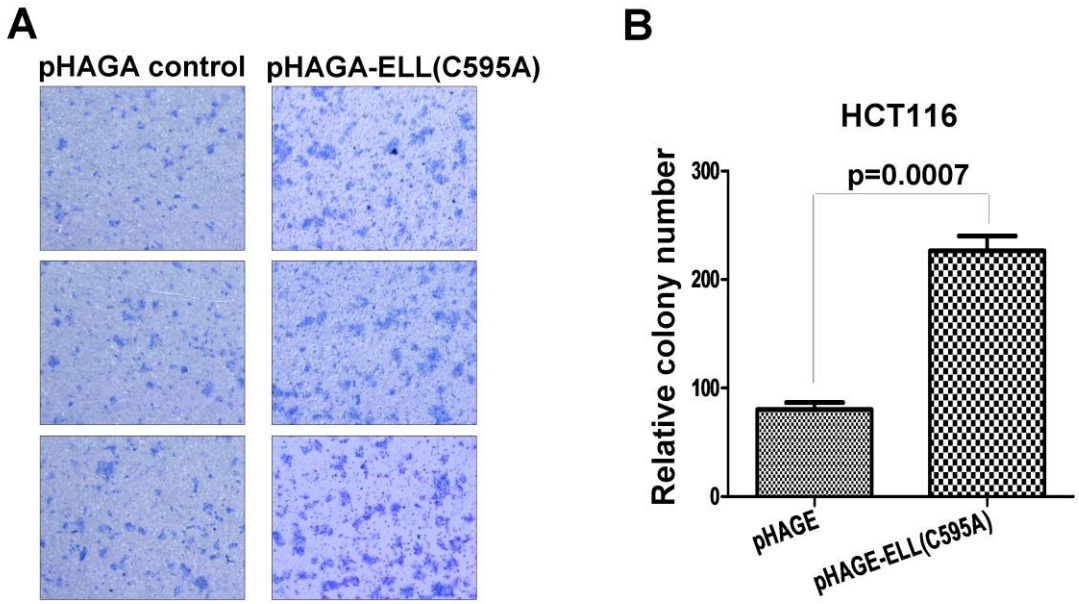


**Supplementary Fig. 14. The ELL(C595A) mutant promotes colon cancer cell invasion.** (A) HCT116 cells with ELL(C595A) expression exhibited higher invasive capability compared to the control HCT116 cells by the cell invasion assays. (B) Quantitative analysis for the cell invasion assays.

**Supplementary Figure 15**

A

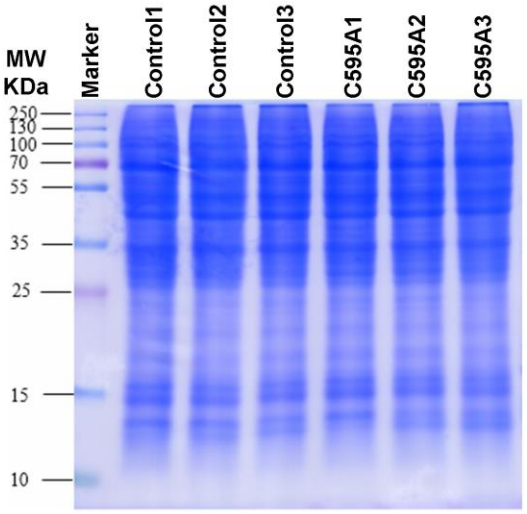


B

The genes up-regulated in the xenograft HCT116 tumors with ELL(C595A) overexpression

| Protein ID | Gene | Up-ratio (>1.2) | P-value (<0.05) |
|---|---|---|---|
| Q9UKX2 | MYH2 | 1.299 | 0.0408497 |
| Q93050 | ATP6V0A1 | 1.221 | 0.0266267 |
| Q96P70 | IPO9 | 1.38 | 0.0208679 |
| P17661 | DES | 1.23 | 0.0222371 |
| Q9BZH6 | WDR11 | 1.2295 | 0.0112769 |
| P49006 | MARCKSL1 | 1.308 | 0.0054785 |
| P50895 | BCAM | 1.301 | 0.0200497 |
| P26447 | S100A4 | 1.213 | 0.0013307 |
| O43688 | PPAP2C | 1.21 | 0.0311648 |
| Q8N684 | CPSF7 | 1.2095 | 0.0048159 |
| O95429 | BAG4 | 1.95 | 0.0190679 |

C

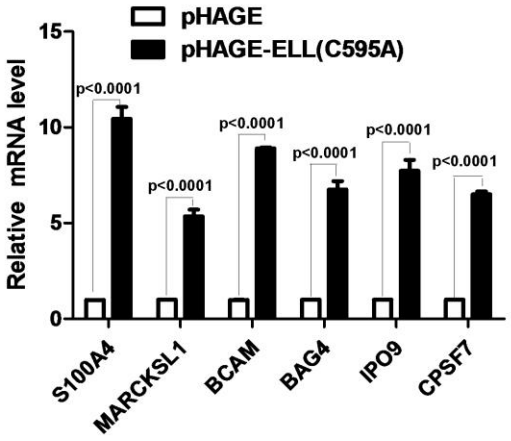


D

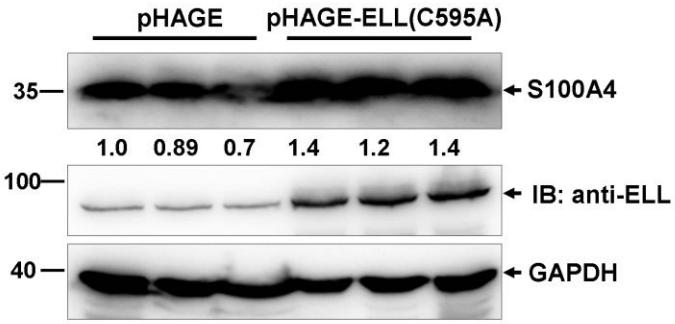


**Supplementary Fig. 15. Quantitative analysis of global proteome in xenograft tumors.** (A) The total proteins used for quantitative proteomics is examined by SDS-PAGE (12%) (each lane loading 30 μg total protein). (B) The genes up-regulated in the xenograft HCT116 tumors with ELL(C595A) overexpression. (C) The up-regulations of genes in the ELL(C595A) xenograft tumors are confirmed by semi-quantitative RT-PCR analysis. (D) The up-regulation of S100A4 in ELL(C595A) xenograft tumors is confirmed by Western Blot analysis.

**Supplementary Figure 16**

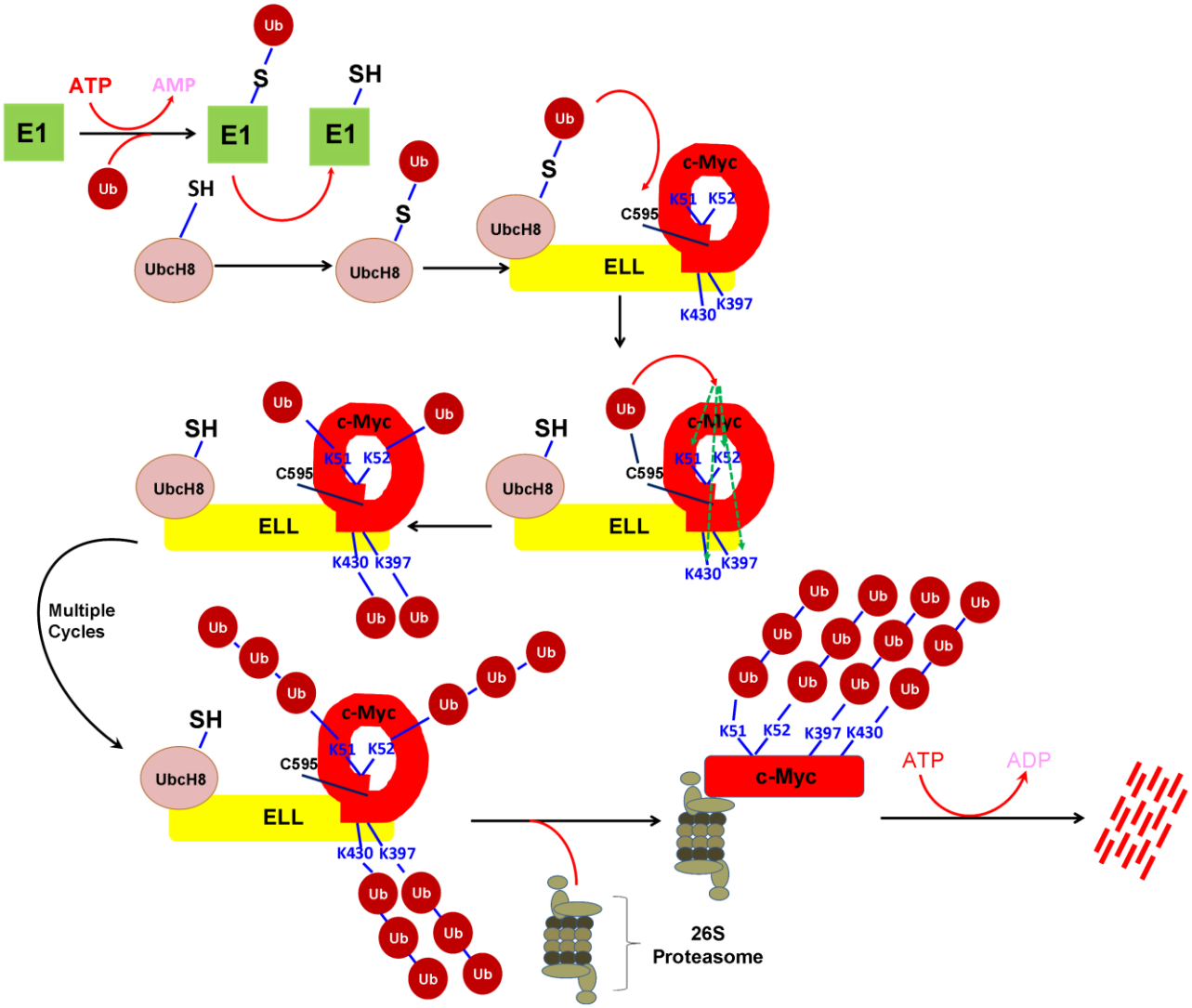


**Supplementary Fig. 16**. **A model of ELL-mediated c-Myc degradation.** UbcH8 transfers ubiquitin to C595 of ELL, after which ELL transfers ubiquitin from C595 to K51/52, K397 and K430 of c-Myc. After multiple cycles, ELL catalyzes the formation of K48-linked polyubiquitin chains at K51/52, K397 and K430 of c-Myc, which are recognized by the 26S proteasome and result in c-Myc degradation.

**Supplementary Figure 17**

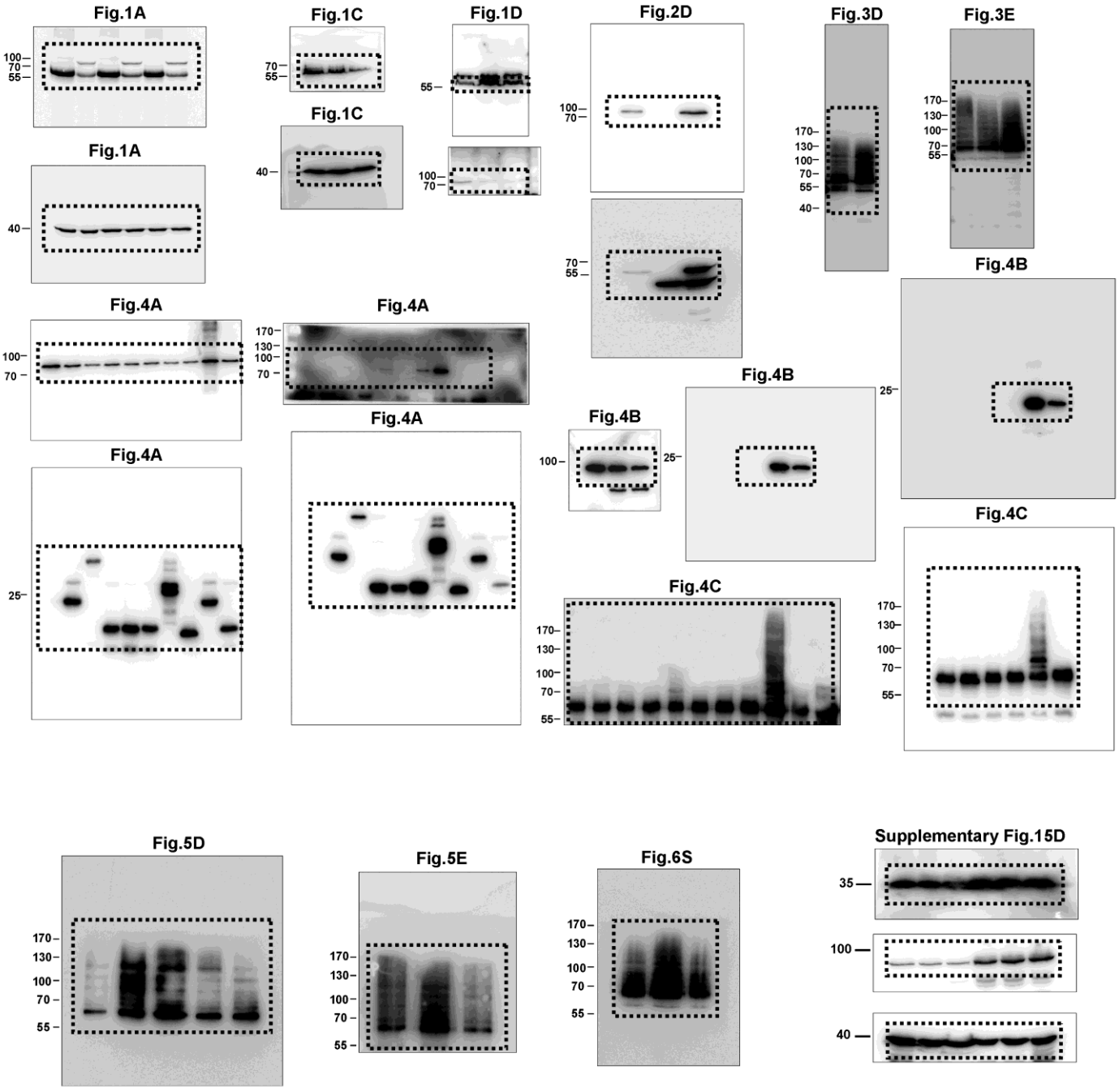


**Supplementary Fig.17. The original full immunoblot images utilized in Figure 1, Figure 2, Figure 3, Figure 4, Figure 5, and Supplementary Figure 15**

**Supplementary Table 1. The primers used for cloning eleven E2 ubiquitin-conjugating enzyme**

| Gene | Sense | Antisense |
|---|---|---|
| UbcH1 | 5’-TCGAATTCCTATGGCCAACATCGC GGTGCAGCGAA-3’ | 5’-TCCTCGAGTCAGTTACTCAGAA GCAATTCT-3’ |
| UbcH2 | 5’-TCAGATCTCTATGTCATCTCCCAGT CCG-3’ | 5’-TACTCGAGCTACAACTCCATATC CT-3’ |
| UbcH3 | 5’-TCAGATCTCTATGGCTCGGCCGCT AGTG-3’ | 5’-TAGCGGCCGCTCAGGACTCCTC CGTGCC-3’ |
| UbcH5a | 5’-TCAGATCTCTATGGCGCTGAAGAG GATT-3’ | 5’-TAGCGGCCGCTTACATTGCATAT TTCTG-3’ |
| UbcH5b | 5’-TCAGATCTCTATGGCTCTGAAGAG AATCC-3’ | 5’-TAGCGGCCGCTTACATCGCATA CTTCT-3’ |
| UbcH5c | 5’-TCAGATCTCTATGGCGCTGAAACG GATTA-3’ | 5’-TAGCGGCCGCTCACATGGCATA CTTCTGAGT-3’ |
| UbcH6 | 5’-TCAGATCTCTATGTCGGATGACGA TTC-3’ | 5’-TAGCGGCCGCTTATGTAGCGTAT CTCT-3’ |
| UbcH7 | 5’-TCGAATTCCTATGGCGGCCAGCAG GAGGCTGAT-3’ | 5’-TAGCGGCCGCTTAGTCCACAGG TCGCTTTTCCCCATAT-3’ |
| UbcH8 | 5’-TCGAATTCCTATGATGGCGAGCAT GCGA-3’ | 5’-TACTCGAGTTAGGAGGGCCGGT CCA-3’ |
| UbcH10 | 5’-TCAGATCTCTATGGCTTCCCAAAA CCGC-3’ | 5’-TAGCGGCCGCTCAGGGCTCCTG GCTGGT-3’ |
| Ubc13 | 5’-TAAGATCTATATGGCCGGGCTGCC CCGC-3’ | 5’-TAGCGGCCGCTTAAATATTATTC ATGGC-3’ |

**Supplementary Table 2. The primers used for confirming gene up-regulation in xenograft HCT116 tumors with ELL(C595A) overexpression by semi-quantitative RT-PCR**

| Gene | Sense | Antisense |
|---|---|---|
| *BAG4* | 5’-TGCACCTGGTTATACTCAGAC C-3 | 5’-TCCATAAGGATAATGGGGCAGGG -3’ |
| *BCAM* | 5’-AGGGCTACATGACCAGCCGC A -3’ | 5’-AGGGCTACATGACCAGCCGCA -3’ |
| *CPSF7* | 5’-TGAGGTGGTGGTAGCCTCTG AA -3’ | 5’-TCACTAGAATCTCGGGAATGGG -3’ |
| *IPO9* | 5’-ACTGAGCACTGGTGGAAGAT CCA -3’ | 5’-GACATAGCAACAGTGAACCGAC -3’ |
| *MARCKSL1* | 5’-CCAACGGCCAGGAGAATGGC CA -3’ | 5’-CTTCTTCTTGGGGGTCTCCT -3’ |
| *S100A4* | 5’-GTGTCCACCTTCCACAAGTA CT -3’ | 5’-TCAGCTTCTGGAAAGCAGCTTC -3’ |